

MIT Open Access Articles

Fusion Yield Enhancement in Magnetized Laser-Driven Implosions

The MIT Faculty has made this article openly available. **Please share** how this access benefits you. Your story matters.

Citation: Chang, P. et al. "Fusion Yield Enhancement in Magnetized Laser-Driven Implosions." Physical Review Letters 107 (2011): n. pag. Web. 19 Oct. 2011. © 2011 American Physical Society

As Published: <http://dx.doi.org/10.1103/PhysRevLett.107.035006>

Publisher: American Physical Society

Persistent URL: <http://hdl.handle.net/1721.1/66505>

Version: Final published version: final published article, as it appeared in a journal, conference proceedings, or other formally published context

Terms of Use: Article is made available in accordance with the publisher's policy and may be subject to US copyright law. Please refer to the publisher's site for terms of use.





Fusion Yield Enhancement in Magnetized Laser-Driven Implosions

P. Y. Chang,^{1,2,3} G. Fiksel,^{1,2} M. Hohenberger,^{1,2,4} J. P. Knauer,² R. Betti,^{1,2,3,4} F. J. Marshall,² D. D. Meyerhofer,^{1,2,3,4}
F. H. Séguin,^{1,5} and R. D. Petrasso^{1,5}

¹*Fusion Science Center, University of Rochester, Rochester, New York 14623, USA*

²*Laboratory for Laser Energetics, University of Rochester, Rochester, New York 14623, USA*

³*Department of Physics and Astronomy, University of Rochester, Rochester, New York 14627, USA*

⁴*Department of Mechanical Engineering, University of Rochester, Rochester, New York 14627, USA*

⁵*Plasma Science and Fusion Center, MIT, Cambridge, Massachusetts 02139, USA*

(Received 11 April 2011; published 15 July 2011)

Enhancement of the ion temperature and fusion yield has been observed in magnetized laser-driven inertial confinement fusion implosions on the OMEGA Laser Facility. A spherical CH target with a 10 atm D₂ gas fill was imploded in a polar-drive configuration. A magnetic field of 80 kG was embedded in the target and was subsequently trapped and compressed by the imploding conductive plasma. As a result of the hot-spot magnetization, the electron radial heat losses were suppressed and the observed ion temperature and neutron yield were enhanced by 15% and 30%, respectively.

DOI: 10.1103/PhysRevLett.107.035006

PACS numbers: 52.57.-z, 52.25.Xz, 52.55.-s

Plasma confinement and the suppression of energy transport are fundamental to achieving the high-energy-density conditions necessary for fusion applications. In the magnetic fusion energy concept [1], this is accomplished by applying strong magnetic fields of the order ~ 0.1 MG, such that the magnetic pressure exceeds the total plasma energy density, i.e., $\beta = 2\mu_0 p/B^2 \ll 1$, with p being the total plasma pressure. Following the formalism developed by Braginskii [2], the electron heat transport is governed by the magnetization parameter $\omega_{ce}\tau_e$, where ω_{ce} is the electron gyrofrequency and τ_e is the electron collision time. Electron confinement and suppression of electron heat conduction are achieved for $\omega_{ce}\tau_e > 1$. Heat-flux suppression is also the basis of magnetized target fusion, where a preformed magnetized plasma is compressed via a cylindrical liner implosion [3], a concept that is being actively pursued both experimentally and analytically (see, e.g., [4]).

Magnetizing the hot spot in an inertial confinement fusion (ICF) implosion can reduce conductive energy transport. This increases the plasma temperature and allows for more fuel to be compressed at lower implosion velocities while still reaching ignition conditions, leading to an improved energy gain [5]. To achieve $\omega_{ce}\tau_e \sim 1$ in the hot spot of a typical direct-drive DT ignition target [6], fields of the order of tens of megagauss are required. Confining α particles generated in the nuclear burn stage, to further reduce energy losses from the hot spot, necessitates fields as high as hundreds of megagauss [7]. Such strong fields are challenging to generate. Magnetic-flux compression, in which an initially lower B field is embedded into a conductor and then compressed, has been shown to be a viable path to tens of megagauss via implosions driven with high explosives and pulsed power sources [8].

Recently, laser-driven magnetic-flux compression has been demonstrated under ICF relevant conditions, with an amplification factor (final field divided by seed field) of $\sim 10^3$, significantly exceeding that of “conventional” compression methods [7,9]. In an ICF target, the shell does not, by itself, trap the enclosed magnetic flux. Instead, upon laser irradiation of the target, the ablation pressure drives a shock wave through the shell, which breaks out into the gas fill inside, thus raising the gas temperature and fully ionizing it. The gas becomes a conductor and traps the magnetic field. Provided that the field diffusion time is longer than the compression time scale, the laser-driven capsule compresses the embedded magnetic flux. For conditions relevant to ICF implosions, the diffusion time has been estimated to be ~ 200 ns, while the implosion time is ~ 4 ns, providing an efficient trapping of the magnetic field [9]. Through simple flux conservation arguments, and taking into account the diffusion of flux into the plasma shell as a result of the finite hot-spot resistivity, the compressed field strength can be expressed as $B_{\max} = B_0(R_0/R)^{2(1-1/R_m)}$. Here R is the hot-spot radius, $R_m \sim 50$ is the time-averaged magnetic Reynolds number, and B_0 and R_0 are the initial seed field and gas fill radius, respectively [9].

In previous laser-driven flux compression experiments using the OMEGA laser [10], a seed magnetic field of 50 kG was trapped and compressed to more than 30 MG in a cylindrical capsule filled with D₂ gas [7,9]. Despite the hot-spot electrons being magnetized under these conditions, no evidence of fusion performance enhancement was observed compared to nonmagnetized implosions. In cylindrical implosions, the hot-spot density increases as $\rho \propto 1/R^2$ (as opposed to $1/R^3$ in spherical implosions), which limits the achievable plasma densities. Consequently, the hot ions most likely to undergo fusion reactions have a mean free path comparable to the hot-spot

radius and undergo only few collisions before leaving the hot spot. Additionally, large shot-to-shot fluctuations caused by target parameter variations (gas pressure, alignment) precluded an accurate assessment of the B -field effects on the target performance [7,9].

This Letter presents experimental results using spherical, magnetized targets that provide a higher hot-spot density and improved shot-to-shot reproducibility. The field compression scales roughly as $1/R^2$, irrespective of a spherical or cylindrical implosion. The experimental results discussed represent the first observation of an enhancement in the ICF performance as a direct result of hot-spot magnetization. Because of the open field-line configuration, the hot-spot thermal losses are only suppressed by $\sim 50\%$. Despite the modest improvement in thermal energy confinement, the enhancements in fusion yields and ion temperatures are clearly detectable. Future experiments will explore closed field-line configurations that are expected to greatly reduce the heat losses.

Figure 1 shows the setup at the center of the OMEGA target chamber. To assess the impact of a magnetized hot spot on an ICF capsule performance, a spherical implosion target is positioned in the center of a single Cu coil. The coil was attached to the magnetized inertial fusion energy delivery system (MIFEDS) device [11], used to drive a 45-kA current with an ~ 350 -ns half-period. It had an inner radius of 3 mm and generated a seed field perpendicular to the coil plane in the \hat{z} direction of $B_0 = 80 \pm 10$ kG across the capsule. This was timed to coincide with the OMEGA laser beams compressing the target. In contrast to previous experiments using a Helmholtz-like coil assembly, the single-coil setup provides stronger magnetic seed fields and minimizes coil interference with laser beam paths. The capsules were CH shells with an outer radius of $430 \mu\text{m}$ filled with 10 atm of D_2 gas. The CH wall thickness, an important parameter for assessing the fuel assembly's performance [12], varied between 23.1 and $24.5 \mu\text{m}$. The coil was in the equatorial plane of the

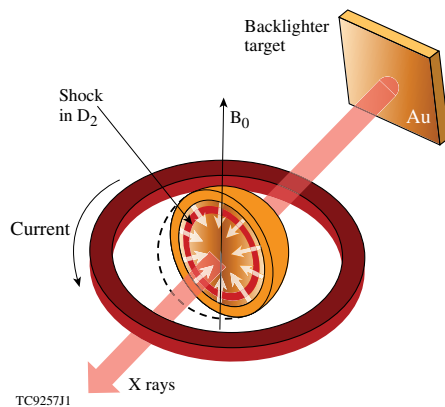


FIG. 1 (color online). A spherical ICF target is placed inside a coil generating an 80-kG magnetic field. The target is imploded by the OMEGA laser, trapping and compressing the field inside. X-ray radiography is used to assess the implosion uniformity.

OMEGA target chamber, blocking 20 OMEGA laser beams from illuminating the target. The remaining 40 beams were repointed using a platform developed for polar-drive (PD) applications [13]. This ensured a target implosion with a high degree of spherical symmetry, even with a nonspherical irradiation pattern [14]. The target was illuminated with 1-ns square laser pulses and a total on-target energy of 18 kJ with an average intensity of $\sim 7 \times 10^{14} \text{ W/cm}^2$. X-ray radiography assessed the implosion uniformity [15]. The x rays were generated by illuminating a $25\text{-}\mu\text{m}$ Au foil mounted 5 mm away from the target at 52.6° off the equatorial plane (see Fig. 1) using four of the remaining OMEGA laser beams. The resulting x rays in the range of 2.5–4.5 keV were imaged onto a fast framing camera [16] after passing through the imploding target. This technique has previously been applied successfully in polar-drive experiments, such as [14]. To assess the target performance, the total neutron yield and the ion temperature were measured using a neutron time-of-flight diagnostic [17], situated 3 m from the target.

The 1D hydrodynamic code LILAC was extended to solve the resistive MHD equations (LILAC-MHD) [18,19] to predict the compressed magnetic field and estimate its effect on the fuel assembly. Applying a 1D simulation to the 3D problem of a magnetic field in a spherically compressed target does not fully capture the nature of the experiment, and extending these calculations to the 3D case will be the subject of future work. Nevertheless, it is possible to investigate characteristics of the B -field compression in a 1D simulation by making the assumptions outlined below. The implosion can be treated as being spherically symmetric since the plasma pressure always exceeds the magnetic contribution ($\beta \gg 1$). Furthermore, the \hat{z} component of the B field was calculated at the target's equatorial plane via the induction equation and then extended over the entire target as a straight solenoidal field. The electron heat conduction is suppressed only perpendicular to the magnetic-field lines. In cylindrical geometry this limitation was alleviated since the target length in the direction of the field significantly exceeded the target diameter; i.e., the field-normal heat loss suppression dominated the uninhibited lateral heat flow. In spherical geometry, the unmodified losses along the field lines must be included to treat the problem correctly. To do this, the total electron thermal conductivity κ_{tot} was treated as a superposition of the parallel and perpendicular contributions, κ_{\parallel} and κ_{\perp} , as $\kappa_{\text{tot}} = \kappa_{\parallel} A_{\parallel} / A_{\text{tot}} + \kappa_{\perp} A_{\perp} / A_{\text{tot}}$. A_{\parallel} and A_{\perp} are the parallel and perpendicular projections of the total hot-spot area A_{tot} . For a spherical hot spot, $A_{\parallel} / A_{\text{tot}} \approx 0.5$, such that even if all perpendicular heat losses are suppressed ($\kappa_{\perp} = 0$), the remaining total loss is reduced by 50% with respect to the unmagnetized case.

Simulation profiles for a spherical implosion using the experimental target and laser parameters and applying the approximations above are shown in Fig. 2. The compressed magnetic-field profile from a $B_0 = 80$ kG seed field

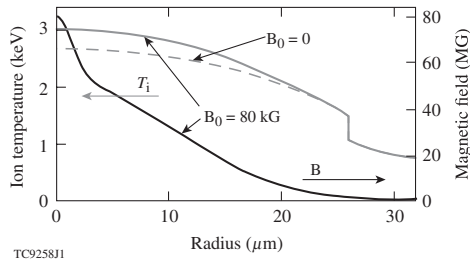


FIG. 2. Compressed magnetic field (solid black) and ion temperature (solid gray) inside a spherical, magnetized hot spot simulated using LILAC-MHD. The ion temperature is enhanced compared to the $B_0 = 0$ case (dashed gray).

(black), the ion temperature using the same seed (solid gray) and without an applied magnetic field (dashed gray) is shown. At this time, the hot-spot radius is $26 \mu\text{m}$ and the field has been amplified to $B_{\text{max}} \approx 80 \text{ MG}$, or a flux-averaged field across the hot spot of $B_{\text{av}} = 15 \text{ MG}$. This compression is consistent with flux conservation and $R_m = 21$, with the theoretical limit in the case of no diffusion ($R_m \rightarrow \infty$) corresponding to a flux-averaged hot-spot field of 19.6 MG . The results in Fig. 2 are not at peak compression. Thus, the field is lower than the experimentally measured field in the cylindrical experiments [7]. Based on these calculations, the expected experimental increase in ion temperature at the target center as a result of a magnetized hot spot is 8%, corresponding to a fusion yield enhancement of 13%. This calculated improvement of the target performance can be attributed solely to the magnetization of the hot spot and does not result from a change of the laser-coupling characteristics (e.g., via modification of the heat transport at the ablation layer). This was confirmed by artificially removing any field effects in the simulation until after the laser had turned off. As expected, no discernible difference was observed compared to calculations with the B -field effects on for the full simulation interval. If the parallel heat losses are suppressed, e.g., by closing the magnetic-field lines, the simulations predict an increase of 42% in the ion temperature and a 73% neutron-yield enhancement. In this case, the target performance is primarily limited by radiative energy losses.

An experimental x-ray backlighter measurement is displayed in Fig. 3, showing an imploded target with and

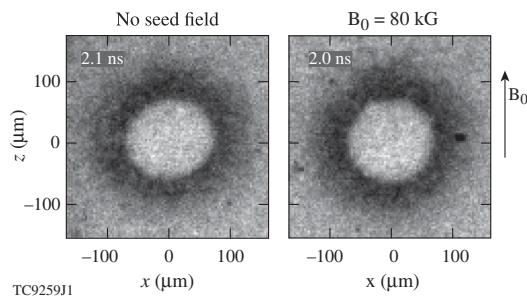


FIG. 3. X-ray backlighter data show no impact by the magnetic seed field on the implosion uniformity.

without an applied seed field and plotted using the same scale and color map. The MIFEDS coil was present around the target in both cases. The data were taken at $\sim 2 \text{ ns}$, a few 100 ps before peak compression. The bright area in the center is the location of the hot spot, the dark region surrounding it results from x rays being absorbed in the dense shell and the coronal plasma. The center appears brighter than the background since the self-emission from the compressed core starts to become brighter than the backlighter emission at this time. The implosion is very uniform, despite using only 40 beams. This confirms the successful application of the PD platform to the magnetic-field compression experiments. No discernible difference is observed between the field and no-field cases, confirming that the magnetic field has no impact on the uniformity of the implosion.

As shown in Ref. [12], the yield of an ICF implosion target decreases with increasing wall thickness. Figure 4 shows the measured neutron yield and the ion temperatures from shots both with an applied seed field of 80 kG (black dots) and without magnetic fields (blue squares) as a function of the target wall thickness. The magnetized target performance is visibly enhanced. To separate the effect of the magnetic field and the wall thickness on the neutron yield Y_n and the ion temperature T_i , a multiple linear regression method expressing these quantities as $Y_n = Y_{n0} + A_B B_0 + A_\Delta \Delta$ and $T_i = T_{i0} + C_B B_0 + C_\Delta \Delta$ is used. B_0 is the seed field (0 or 80 kG) and Δ denotes the shell thickness. A least-squares fit to the data yields the fitting parameters listed in Table I, giving the yield in units of 10^9 and the temperature in keV. The goodness of the fit is assessed with an F test that equates to a degree of confidence in the model of better than 94%. The result of the linear regression method is plotted as the solid ($B_0 = 80 \text{ kG}$) and dashed ($B_0 = 0$) lines in Fig. 4, showing a clear enhancement of both the neutron yield as well as the ion temperature. For shots where the magnetic seed field was applied, the yield was enhanced by 30%, the ion temperature by 15%. The overall scatter of data points

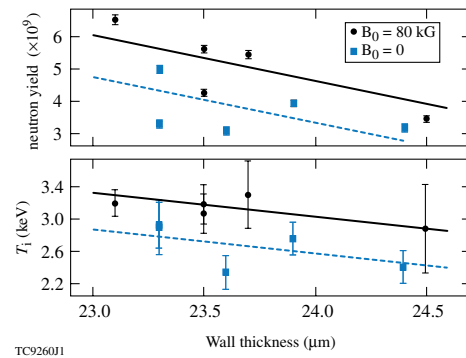


FIG. 4 (color online). Experimental neutron yield and ion temperature plotted against target wall thickness. A clear enhancement of the magnetized implosions (black dots) compared to the $B_0 = 0$ case (blue squares) is observed. The lines are fits to the data using the parameters listed in Table I.

TABLE I. Multiple linear regression coefficients for the fits to the experimental data in Fig. 4.

	Y_{n0} , T_{i0}	A_B ($10^{-5}/\text{G}$), C_B ($10^{-6}/\text{G}$)	A_Δ ($1/\mu\text{m}$), C_Δ ($1/\mu\text{m}$)
Y_n ($\times 10^9$)	37.6	1.7 ± 0.6	-1.4 ± 0.6
T_i (keV)	8.57	4.8 ± 1.3	-0.25 ± 0.11

for measurements with a magnetic field appears to be reduced compared to the no-field measurements. The data shown in Fig. 4 represent the first measurement of a fusion performance enhancement resulting from embedding a strong magnetic field into an ICF capsule.

In previous experiments the compressed magnetic field was determined via proton deflectometry [7,9]. The single coil used here blocked the line of sight through the target perpendicular to the field, preventing the use of a proton probe. To confirm the flux amplification in spherical implosions, the single coil was exchanged with a Helmholtz coil, as used in [7], while a glass sphere filled with D^3He gas and imploded using 12 OMEGA beams was used as an $\sim 15.2\text{-MeV}$ proton source. The protons traversing the target were deflected by the magnetic field and recorded on a CR39 track detector with the deflection pattern giving information about field topology and magnitude. This has been shown to result in a characteristic two-peak structure [7,9]. Protons traversing the compressed hot-spot field ($\sim 30\text{ MG}$) provide a strongly deflected peak, while protons propagating through the target wall experience a lower field ($\sim 1\text{ MG}$) and are weakly deflected but produce a higher-amplitude peak. Given the hot-spot size, the number of protons interacting with a spherical hot spot was lower than in the cylindrical case, thus decreasing the signal-to-noise ratio. Indeed, so far it has not been possible to obtain an unambiguous spherical hot-spot field measurement by observing a strongly deflected peak. Figure 5 shows a proton density lineout across a CR39 detector for $\sim 14.8\text{-MeV}$ protons that have slowed down in the dense shell. A strong peak is visible to the right of the hot spot (positioned at zero) caused by deflection in the target shell. While this does not provide the hot-spot field amplitude as discussed above, it is a signature of the magnetic field being trapped and amplified in the target and confirms the presence of a strong magnetic field inside the capsule.

In summary, a seed magnetic field of about 80-kG strength was embedded into spherical ICF targets imploded by the OMEGA laser in a PD beam-pointing geometry. As a result of the high implosion velocities and ionization of the target gas fill, the magnetic field inside the capsule was trapped and amplified through magnetic-flux compression, with simulations indicating a flux-averaged hot-spot field of 15 MG at peak neutron yield. The implosion was confirmed to be spherically uniform by using x-ray radiography, showing no discernible difference in core symmetry with and without an applied seed field. At the strong magnetic fields reached in these experiments,

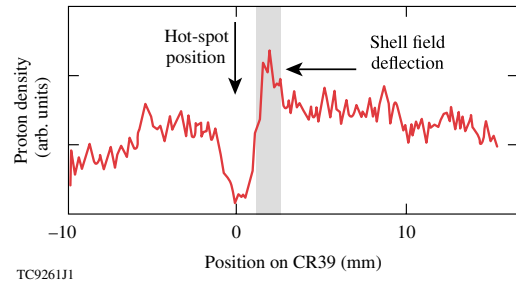


FIG. 5 (color online). The cross-core proton deflectometry lineout exhibits a one-sided peak from protons traversing the magnetized target shell—a signature of a compressed B field inside the capsule.

the hot spot inside a spherical target becomes strongly magnetized, suppressing the heat losses by about 50% through electron confinement. As a result, the experimentally measured ion temperature and fusion yield were improved by 15% and 30%, respectively. This is in qualitative agreement with results from 1D LILAC-MHD calculations, giving 8% and 13%, respectively. The difference can be attributed to the limited applicability of a 1D code to the inherently 3D problem of the magnetic field in a spherically compressed target. Extending these calculations to three dimensions will be the subject of future work. The data discussed here represent the first experimental verification of an ICF target performance being enhanced by magnetizing the hot spot.

This work has been supported by the U.S. Department of Energy under Cooperative Agreement No. DE-FC02-04ER54789 and No. DE-FC03-92SF19460.

- [1] J. A. Wesson, *Tokamaks* (Clarendon Press, Oxford, 2004).
- [2] S. I. Braginskii, in *Reviews of Plasma Physics*, edited by M. A. Leontovich (Consultants Bureau, New York, 1965).
- [3] R. C. Kirkpatrick, I. R. Lindemuth, and M. S. Ward, *Fusion Technol.* **27**, 201 (1995).
- [4] T. Intrator *et al.*, *Phys. Plasmas* **11**, 2580 (2004); S. A. Slutz *et al.*, *Phys. Plasmas* **17**, 056303 (2010).
- [5] R. Betti and C. Zhou, *Phys. Plasmas* **12**, 110702 (2005).
- [6] P. W. McKenty *et al.*, *Phys. Plasmas* **8**, 2315 (2001).
- [7] O. V. Gotchev *et al.*, *Phys. Rev. Lett.* **103**, 215004 (2009).
- [8] A. D. Sakharov, *Sov. Phys. Usp.* **9**, 294 (1966); F. S. Felber *et al.*, *Phys. Fluids* **31**, 2053 (1988).
- [9] J. P. Knauer *et al.*, *Phys. Plasmas* **17**, 056318 (2010).
- [10] T. R. Boehly *et al.*, *Opt. Commun.* **133**, 495 (1997).
- [11] O. V. Gotchev *et al.*, *Rev. Sci. Instrum.* **80**, 043504 (2009).
- [12] F. J. Marshall *et al.*, *Phys. Plasmas* **7**, 1006 (2000).
- [13] F. J. Marshall *et al.*, *J. Phys. IV (France)* **133**, 153 (2006).
- [14] F. J. Marshall *et al.*, *Phys. Rev. Lett.* **102**, 185004 (2009).
- [15] O. L. Landen *et al.*, *Rev. Sci. Instrum.* **72**, 627 (2001).
- [16] D. K. Bradley *et al.*, *Rev. Sci. Instrum.* **66**, 716 (1995).
- [17] R. A. Lerche *et al.*, *Rev. Sci. Instrum.* **66**, 933 (1995).
- [18] J. Delettrez *et al.*, *Phys. Rev. A* **36**, 3926 (1987).
- [19] N. W. Jang *et al.*, *Bull. Am. Phys. Soc.* **51**, 144 (2006).